

# Response of surface energy components to urban heatwaves and its impact on human comfort in coastal city

Yizhao Wei <sup>a,1</sup>, Han Chen <sup>a,1</sup>, Jinhui Jeanne Huang <sup>b,\*</sup>

<sup>a</sup> College of Environmental Science and Engineering/Sino-Canada Joint R&D Centre for Water and Environmental Safety, Nankai University, Tianjin 300071, PR China

<sup>b</sup> Shenzhen Research Institute of Nankai University, Shenzhen 518057, China



## ARTICLE INFO

### Keywords:

Heatwave  
Sensible heat flux  
Latent heat flux  
Human comfort  
Urbanization  
Stomatal process-based urban energy balance model

## ABSTRACT

Heatwaves become more intensive and frequent due to global warming, but their impact on energy components, such as sensible heat flux and latent heat flux, and human discomfort remains unclear. This study combines the discomfort index and the Excess Heat Factor to estimate the Excess Discomfort Factor, an index that reflects the degree of human comfort during a heatwave. The daily energy components are reconstructed before and during heatwave events in Shenzhen, China using a stomatal process-based urban energy balance model from 1980 to 2019. The effects of heatwaves on changes in the energy components of different urban surfaces (i.e. soil, vegetation, impervious surfaces, and water bodies) are analyzed, and their impact on human comfort is further investigated. During the heatwave, vegetation was found to be more effective in regulating human comfort compared to water bodies. However, urbanization has reduced the capacity of vegetation to regulate human comfort during the heatwaves by 22.5% over a 40-years period. Furthermore, the changes in energy components in impervious surfaces best reflect the degree of human discomfort during a heatwave. Overall, this research enhances our understanding of the response of surface energy components to urban heatwaves and their relationship with human comfort.

## 1. Introduction

A heatwave is characterized by an extended period of exceptionally high temperatures. In China, the definition endorsed by the China Meteorological Administration has gained widespread acceptance, stipulating a daily maximum temperature exceeding 35 °C for a duration of at least three consecutive days (Xu et al., 2016). The exacerbation of heatwaves in China traces back to 1960, with regional occurrences nearly doubling in both frequency and intensity compared to the levels observed in 1960, as of 2018 (Wang and Yan, 2021; He et al., 2022; He, 2023). Heatwaves can impact various industries, including livestock, fisheries, tourism, utilities, and construction (Ahmed et al., 2023; Li et al., 2023; Wang et al., 2023). Previous research reported that heatwaves lead to increased mortality rates from various diseases, including cardiovascular (Zhou et al., 2023), respiratory (Szagri et al., 2023), mental and neurological (Zhang et al., 2023); diabetes (Moreno-Fernandez et al., 2023); and renal and urological diseases (Conti et al., 2007;

\* Corresponding author at: Sino-Canada R&D Centre on Water and Environmental Safety, College of Environmental Science and Engineering, Nankai University, Tianjin 300071, PR China.

E-mail address: [huangj@nankai.edu.cn](mailto:huangj@nankai.edu.cn) (J.J. Huang).

<sup>1</sup> These authors contribute equally to this article.

Huang et al., 2023a, 2023b).

Heatwaves are linked to high-pressure areas, atmospheric blocking patterns, reduced cloud cover, and warm air advection prior to their occurrence (García-A-Herrera, 2010; Barriopedro et al., 2011; Liang et al., 2022). From the perspective of surface energy balance, the continuous release of latent heat flux before a heatwave depletes moisture from the soil, resulting in the accumulation of sensible heat flux (Mazdiyasni and Aghakouchak, 2015). When extreme heatwave events occur, the soil surface is dry, and the sensible heat flux significantly increases. This depletion of surface soil moisture and reduction in evaporative cooling effect can further elevate the air temperature (Teuling et al., 2010; Miralles et al., 2012; Miralles et al., 2014). Overall, heatwave events are closely correlated to changes in meteorological factors such as wind speed, pressure, and temperature, as well as changes in energy balance (i.e. net radiation flux, sensible heat flux, and latent heat flux) prior to their occurrence (Kong et al., 2023; Xu et al., 2023). In urban environments, natural land surfaces are supplanted by buildings and roads, resulting in the modification of surface attributes, including albedo, vegetation fraction, and roughness length. These alterations exert a discernible influence on the dynamic interplay between the urban surface and the atmosphere, culminating in shifts in energy exchange patterns. Benson Lira et al. utilized weather research and forecasting (WRF) systems to identify the most significant thermal changes occurring during the urbanization process of the Mexico City Metropolitan Area. It was found that the prominent heat variations manifested during daytime, with a substantial increase of over 4 °C observed in the near-surface air temperature. The urban heat island phenomenon refers to the situation where urban areas are warmer than the surrounding rural areas (He et al., 2020a). During urban heat island, different urban surfaces (impervious, vegetation, water) exhibit distinct energy response mechanisms (Zou et al., 2021). The changes in latent and sensible heat fluxes induced by urbanization are more pronounced during heatwave occurrences (He et al., 2020a, 2020b; Ma et al., 2024). Some studies have also identified diverse interactions between different land use types and heatwaves (Jiang et al., 2019; Chew et al., 2021). Nevertheless, these distinctions have been predominantly qualitative in nature and lack systematic analysis.

The surface energy component flux has a significant impact on human comfort (Jung et al., 2019; Sinha et al., 2022; Di Bernardino et al., 2023). When there is a significant disparity in energy fluxes before and during the occurrence of a heatwave, it signifies a substantial impact of the heatwave on the Earth's surface. This indirectly reflects the intensity of the heatwave from a surface energy perspective (Kong et al., 2023). If a specific surface exhibits a substantial difference in energy fluxes before and during a heatwave event, but the human comfort during the heatwave remains high, it indicates a strong regulatory capacity of that surface in maintaining human comfort during the heatwave (Huang et al., 2023a, 2023b). Thus, the relationship between the energy flux differential before and during a heatwave and human comfort during the heatwave signifies the regulatory capacity of a surface in maintaining human comfort during such events. With the ongoing process of urbanization and global climate warming, temperatures at meteorological stations within urban areas are annually surpassing new extremes (Tripathy and Mishra, 2023). During this process, the regulatory capabilities of different urban surfaces on human thermal comfort during heatwaves warrant exploration. The Excessive Heat Factor (EHF) is the most commonly used index for quantifying human comfort during heatwaves (Piticar et al., 2018). The EHF has a significant advantage in analyzing heatwave-related mortality and morbidity compared with the daily maximum temperature (Langlois et al., 2013; Scalley et al., 2015; Hatvani-Kovacs et al., 2016). However, the EHF calculation only uses temperature as an indicator to characterize heat stress. Physiological heat stress is related to various meteorological elements such as air temperature, relative humidity, and wind speed (Becker et al., 2003). Thom's Discomfort Index (DI) is a widely-used metric in urban climate studies that characterizes the degree of human thermal sensation in urban areas (Zauli Sajani et al., 2008; Da Silva et al., 2010). The DI expands on EHF provides a more comprehensive representation of human comfort during heatwave events.

To enhance the understanding of the response of urban energy changes and human comfort to heatwave events, this study aims to: (1) develop a model for producing a daily-scale retrieval model of energy components to study the changes in energy before and during heatwave; (2) conduct a statistical analysis of the temporal characteristics of heatwaves (duration of heatwaves and human comfort) in Shenzhen over the past 40 years (1980–2019); (3) analyze the impact of heatwaves on the energy balance of different urban surfaces; and (4) reveal the effect of energy changes before and during heatwave occurrences on human comfort in the context of urbanization.

## 2. Data and methods

### 2.1. Identification of heatwave events

In this study, a heatwave is characterized as a period during which the daily maximum temperature surpasses 35° Celsius for more than 3 consecutive days, identifying this interval as a heatwave event. This definition, advocated by the China Meteorological Administration (CMA), has gained widespread acceptance for delineating heatwaves in China (Xu et al., 2016).

### 2.2. Study area

Shenzhen is a coastal city located in southern China (longitude: 113°46' ~ 114°37'; latitude: 22°27' ~ 22°52'), has a subtropical monsoon climate characterized by long summers and short winters, mild temperatures, ample sunshine, and abundant rainfall. The annual average temperature is 23.3 °C, with the lowest average temperature occurring in January of 15.7 °C, and the highest average temperature in July of 29.0 °C. Shenzhen experiences an average of 1853.0 annual sunshine hours and an average annual precipitation of 1932.9 mm (data obtained from the Meteorological Bureau of Shenzhen Municipality, [www.weather.sz.gov.cn](http://www.weather.sz.gov.cn)). More than 60% world's population lives in coastal areas within a 100 km radius. The high population density and elevated relative humidity make people in coastal area more vulnerable to the heatwaves. Shenzhen, the fastest-growing city located on the southeast coast of China, has experienced significant urbanization since the establishment of the special economic zone in 1980. From 1980 to 2020, the

population of Shenzhen grew from 314,100 to 17.56 million, representing a staggering 55-fold increase. Concurrently, the urbanization rate in Shenzhen rose from 4.12% to 39.14%, an almost tenfold increase.

The Yangmeikeng Flux Monitoring Station (Ymk Station) is located on the east coast of Shenzhen at coordinates  $114^{\circ}35'9''E$  and  $22^{\circ}32'29''N$ , with an elevation of 115 m above sea level. The Chi'ao Reservoir Flux Monitoring Station (Ca Station) is located in the central region of Shenzhen at coordinates  $114^{\circ}22'1''E$  and  $22^{\circ}39'51''N$ , with an elevation of 15 m above sea level. The monitoring equipment at Ymk and Ca stations primarily comprises the Eddy Covariance Technique (EC) and micro-meteorological stations. The data monitored predominantly include sensible heat flux, latent heat flux, carbon dioxide flux, wind speed, air temperature, humidity, atmospheric pressure, and radiation. The validation of remote sensing models in this study is primarily reliant on the data provided by Ymk and Ca stations (Fig. 1). (See Table 1.)

### 2.3. Human comfort parameters in heatwaves

Thom's DI takes into account the combined impact of air temperature and relative humidity on human comfort, allowing for an accurate assessment of comfort conditions in outdoor spaces. Thom's DI is calculated by the following equation:

$$DI = T_a - 0.55(1 - 0.01RH)(T_a - 14.5) \quad (1)$$

where  $T_a$  is the mean daily air temperature ( $^{\circ}C$ ) and  $RH$  is the mean daily relative humidity (%). Thom's DI has been widely used in urban planning and design to improve outdoor thermal comfort for pedestrians, tourists and workers.

In this study, the temperature component in EHF calculations is replaced by the DI. The constructed Excess Discomfort Factor (EDF) offers a more comprehensive representation of human comfort during heatwave periods.

The Significance Excess Discomfort Index ( $EDI_{sig}$ ), which quantifies the environmental discomfort load, is calculated using Eq. (2). Temperature and humidity data from ERA5-land for Shenzhen, covering the period from 1980 to 2019, were utilized to calculate the 95th percentile of the Daily DI ( $DI_{95}$ ), serving as the reference climatic value. The capacity of local communities to adapt to heat stress during a heatwave is encapsulated by the  $EDI_{sig}$  (Nairn and Fawcett, 2015; Rohini et al., 2016; Loughran et al., 2017). The Acclimatisation Excess Discomfort Index ( $EDI_{accl}$ ) is defined as the difference between the average DI during a heatwave and the average DI for the 30 days prior to the heatwave.  $EDI_{accl}$  represents a period of heat that is warmer, on average, than the recent past.

$$EDI_{sig} = \left[ \sum_{i=1}^n DI_i / n \right] - DI_{95} \quad (2)$$

$$EDI_{accl} = \left[ \sum_{i=1}^n DI_i / n \right] - (DI_{i-1} + DI_{i-2} + DI_{i-3} + \dots + DI_{i-30}) / 30 \quad (3)$$

$$EDF = EDI_{sig} \times EDI_{accl} \quad (4)$$

$n$  represents the duration of the heatwave in days.  $DI_i$  denotes the average DI on the  $i$ -th day of the heatwave occurrence, while  $DI_{i-a}$  represents the average DI on the  $a$ -th day before the onset of the heatwave. The  $DI_{95}$  denotes the 95th percentile of the historical daily discomfort index in this region.

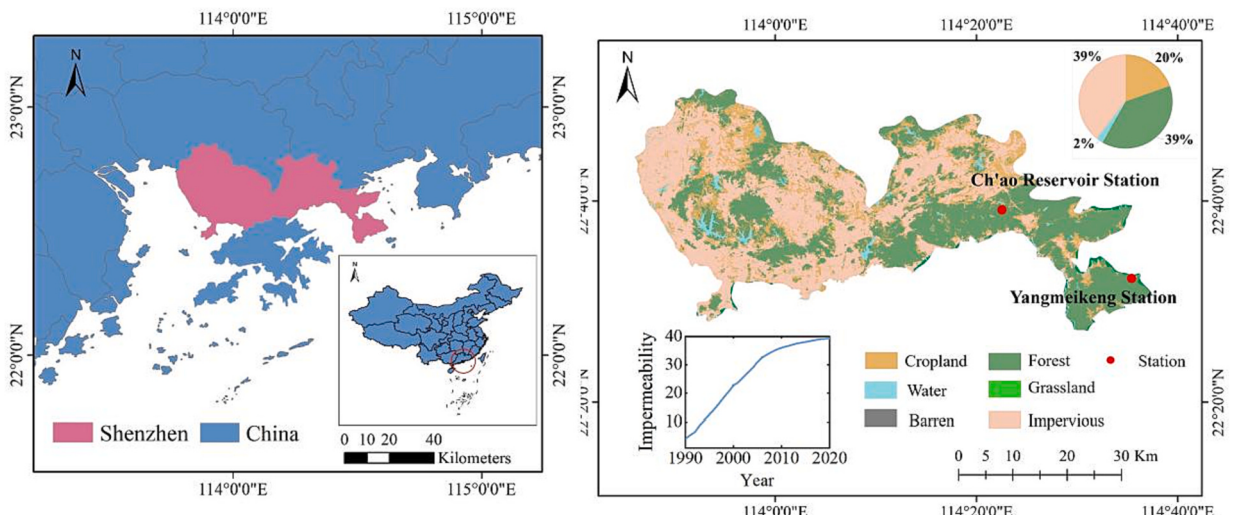


Fig. 1. (a) Geographic location of the study area; (b) Land-use division and proportion of each land cover for the study area.

**Table 1**

Selected 6 typical heatwave events.

Year Division	Heatwave Occurrence Time	UI(%)	EDF	Levels
Around 1980	1991/6/1	5.4	2.552	High
	1986/8/26	4.0	0.097	Low
Around 2000	2004/6/27	27.2	1.593	High
	2003/8/9	28.9	0.101	Low
Around 2019	2018/5/28	39.0	1.122	High
	2019/8/19	39.1	0.013	Low

UI indicates urban impermeability.

#### 2.4. Urban four-source energy balance model

Chen et al. (2022) developed an urban four-source energy balance model (FSU model) to estimate urban evapotranspiration and its components (soil evaporation, vegetation transpiration, impervious surface evaporation and water body evaporation). The FSU model classifies urban areas into three types of surface conditions: permeable areas (such as woodlands, farmland, wetlands, grasslands, and gardens), impervious areas (such as roads and buildings), and water bodies. However, obtaining daily land surface temperature is challenging due to the limitations of satellite revisit periods. To address this issue, the study modified the FSU model by only using meteorological variables to calculate the stomatal resistance. The daily energy components are reconstructed using the stomatal process-based urban energy balance model (SUE model) to analyze changes in the energy components before and during the heatwave events.

The SUE model utilizes a combination of the “patch” and “layer” conceptualizations to simulate energy balances in urban areas. The SUE model assumes that the three types of urban surfaces have independent energy balances and water vapor diffusion processes, neglecting the coupling effect between each patch in the energy balance simulation (Lhomme et al., 2012). The “patch” method is used in the energy balances simulation of different urban land uses, while the “layer” method is used to characterize the two primary sources of energy (i.e. a substrate (bare soil or grass) and an upper canopy (main foliage)). The SUE model is a novel approach that combines the strengths of both “patch” and “layer” conceptualizations to improve the accuracy of energy balances estimation in urban areas (Lhomme et al., 2012; Jingyi et al., 2021). The expression of the SUE model is shown as Eq. (5).

$$LE_{veg} = LE_{soil} + LE_{veg\_canopy} = \frac{\Delta R_n F_c + \rho C_p (e_s - e_a) / r_{ah}}{\Delta + \gamma \left( \frac{r_{s,v}}{r_{ah}} \right)} + \frac{\Delta R_n (1 - F_c) + \rho C_p (e_s - e_a) / r_{ah}}{\Delta + \gamma \left( \frac{r_{s,s}}{r_{ah}} \right)} \times \left( \frac{RH}{100} \right)^{(e_s - e_a)/100} \quad (5)$$

where  $LE_{veg}$  is the total latent heat flux of vegetation,  $LE_{soil}$  is the latent heat flux of soil, and  $LE_{veg\_canopy}$  is the latent heat flux of vegetation canopy;  $R_n$  is the net radiant flux ( $\text{W}/\text{m}^2$ );  $F_c$  is the fractional vegetation coverage;  $C_p$  represents the specific heat of constant pressure ( $\text{J}/\text{kg}/\text{K}$ );  $\gamma$  represents the constant of psychrometric ( $\text{kPa}/\text{K}$ );  $r_{ah}$  represents the aerodynamic resistance ( $\text{s}/\text{m}$ ),  $r_{s,v}$  represents the soil boundary layer resistance ( $\text{s}/\text{m}$ ).  $e_s$  is the saturation water vapor pressure ( $\text{hPa}$ );  $e_a$  is the atmospheric water vapor pressure ( $\text{hPa}$ ). The latent heat fluxes for the impervious surface is calculated as follows (Wong et al., 2015):

$$LE_{imp} = \frac{\rho C_p}{\gamma} \frac{e_s^* - e_a}{r_{ah\_imp} + r_{s\_imp}} \quad (6)$$

where  $r_{s\_imp}$  is the surface resistances of the impervious surface ( $\text{s}/\text{m}$ ).  $LE_{imp}$  tends to be zero in a dry midday. The evaporation from open water body is estimated using Eq. (7). The Penman equation and its variants (e.g., the Penman-Monteith equation) has been widely applied for potential evaporation and water body evaporation estimations (McMahon et al., 2013; Zhao and Gao, 2019).

$$LE_{water} = \frac{\Delta R_n + \gamma f(u)(e_s - e_a)}{\Delta + \gamma} \quad (7)$$

where  $f(u)$  is the wind function which aims to characterize the convection effect. When air moves from land to the water body, the humidity above the water body gradually increases due to evaporation loss. As a result, evaporation fluxes decrease in the downwind direction due to the increased humidity. Therefore, a universal wind function is necessary for simulating evaporation from a water body in urban areas. The improved wind speed function takes into account the effect of relative humidity changes when air moves from the land surface to the water body, shown as follows:

$$f(u) = \gamma(2.33 + 1.65u)L_f^{-0.1} \quad (8)$$

#### 2.5. Remote sensing and meteorological data source

We analyze the temporal characteristics of heatwave events over a 40-years period (1980–2019) using satellite observations, meteorological factors, and auxiliary data. The urban land use data is obtained from the Chinese Land Cover Dataset (CLCD), specifically the first annual dataset, which is generated at the Google Earth Engine (GEE) platform using Landsat observations (Yang and

Huang, 2021). The surface biophysical parameters such as the Normalized Difference Vegetation Index (NDVI) and impervious surface cover (ISC) are derived from Landsat imagery with a spatial resolution of 30 m. NDVI is calculated using the near-infrared and infrared bands of Landsat 4, 5, and 8 satellites. Meteorological Bureau of Shenzhen Municipality specifies that the summer season is from April 20 to November 7, which is very long in Shenzhen. Due to the recurrence period of satellite and the presence of cloud cover in Landsat images, two NDVI measurements are required for Shenzhen per year. One NDVI is the average of all available Landsat images in summer season and another is all available Landsat images in the remain three seasons. This ensure that there are two NDVIs of the whole area that can be used in the model calculation each year.

ERA5-Land is a reanalysis dataset that is generated by replaying the terrestrial component of the European Centre for Medium-Range Weather Forecasts (ECMWF) ERA5 climate reanalysis. The reanalysis dataset combines modelling data with observation data based on the physics laws across the global scale. The various meteorological factors, including dewpoint temperature, air temperature, net solar radiation, surface pressure, and wind speed, are directly obtained from the ERA5-Land dataset for 119 heatwave events (Hersbach et al., 2020). The resolution of the dataset is  $0.1^\circ$ , equivalent to 9 km. The daily DI and EDF for each heatwave event during the period from 1980 to 2019 were calculated by inputting the daily average temperature and average dew point temperature into Eqs. (1)–(4). These meteorological factors are also utilized as inputs for the SUE model to calculate changes in the energy balance components before and during the heatwave event. The extraction and pre-processing of meteorological data based on ERA5-Land are performed using the Google Earth Engine (GEE). Before commencing calculations, interpolation, resampling, and clipping procedures were executed in the ArcGIS software to standardize the spatial resolution of all input data to 30 m. The resampling method utilized in ArcGIS was CUBIC.

## 2.6. Model evaluation and implementation

To validate the performance of the SUE model, the daily latent and sensible heat fluxes are monitored at Ymk Station and Ca Station during the period 2020 to 2021. The RMSE (root mean square error) and  $R^2$  (coefficient of determination) are selected as metrics (Fig. 2). Generally, the SUE model can provide reliable estimates of the energy components according to the ground verification results. The SUE model is used to calculate the daily energy components for each 119 heatwaves (30 days prior to the heatwave to its end) in Shenzhen.

By comparing the average surface energy components during the 30 days before the heatwaves with those during the heatwave event, this study examined the changes in surface energy components before and during heatwaves. For instance, the average energy components during the 30 days before the occurrence of heatwaves at vegetated urban surfaces is calculated using Eq. (9).

$$EC_{mean\_dur30dbHw} = (EC^{-1}_{mean} + EC^{-2}_{mean} + \dots + EC^{-30}_{mean}) / 30 \quad (9)$$

where  $EC_{mean}^n$  represents the average energy for the vegetation surface on the  $n_{th}$  day before the occurrence of the heatwave. Assuming that the heatwave lasts for  $n$  days, the average energy during the occurrence of a heatwave on a vegetated urban surface can be calculated using Eq. (10).

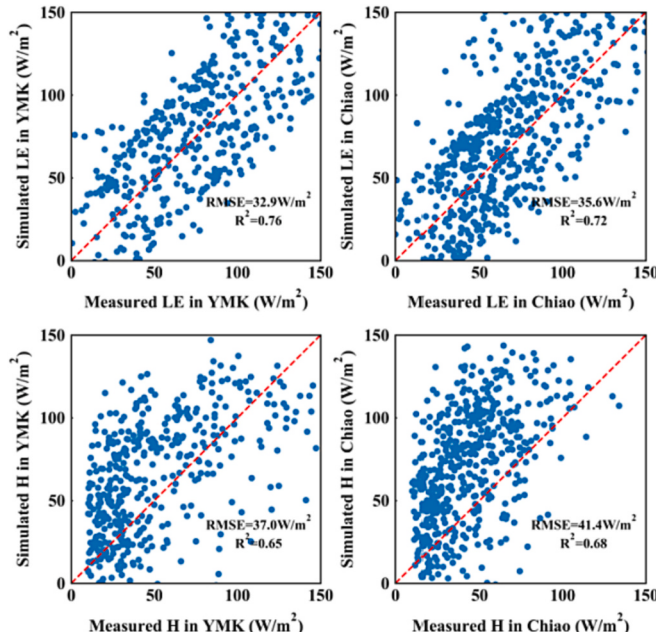


**Fig. 2.** Scatter plot of simulated and measured two energy components (LE and H) from 2020 to 2021 for two sites (Ymk Station and Ca Station).

$$EC_{mean\_durHw} = (EC^1_{mean} + EC^2_{mean} + \dots + EC^n_{mean})/n \quad (10)$$

$EC_{mean}$  represents the average energy components for the vegetation surface on the  $n$ th day of the heatwave. The difference in average energy components during the heatwave and the 30 days prior ( $\Delta EC$ ) can be calculated using Eq. (11).

$$\Delta EC = EC_{mean\_durHw} - EC_{mean\_durdBHW} \quad (11)$$

### 3. Results and analysis

#### 3.1. Shenzhen heatwave event statistics

We analyzed the temporal characteristics of heatwaves in Shenzhen, focusing on 119 heatwave events that occurred during the period of 1980 to 2019 (Fig. 3). Fig. 3(b) illustrates the temporal variations in the number of annual heatwaves in Shenzhen from 1980 to 2019. The number of annual heatwaves (NA) exhibits a close relationship with the annual heatwave intensity. From 1980 to 1985, NA generally remained below two. However, during the period of 1985 to 1990, NA consistently reached at least three, with the exception of a single heatwave event in 1992. From 1995 to 2010, NA consistently remained at a minimum of three, with the extreme years of 1990 and 2000 recording six and five heatwave events, respectively. Notably, post-2010, there is an increase in NA, reaching a peak of eight in 2019, closely approaching the highest number recorded during the period from 1980 to 2019. Fig. 3(c) shows the number of monthly heatwave events that occurred from 1980 to 2019. Heatwaves in Shenzhen mainly occurred in the five months from May to September. Most of heatwaves concentrated in June to August, and the largest number of heatwaves occurred in September.

Fig. 3(d) shows that the intensity and month range of heatwaves have increased in recent years. According to the auxiliary lines in Fig. 3(d), the month range of heatwave occurrences has expanded over the 40-years period. In the early 1980s, heatwaves occurred only in late June and early August. However, around 2000, the heatwaves gradually expanded to cover the period from early June to late September. In recent years, heatwave events have expanded further, occurring from May to the end of September. In fact, the last heatwave in 2019 even occurred on September 30. The strongest heatwave in the EDF occurred on May 1, 1990, with an intensity value of 2.5.

Days of the heatwave lasted (DHL) has a significant impact on human comfort. Fig. 3(e) displays the distribution of DHL in Shenzhen over the past 40 years. The results indicate that DHL was generally below five days before 1990 and gradually increased to seven days after 1990. The longest DHL during the analysis period occurred on May 1, 2000. After the DHL peak in 2000, the average DHL exhibited a smoother temporal pattern. The DHL gradually stabilized at about four days from 2005 to the present. However, the

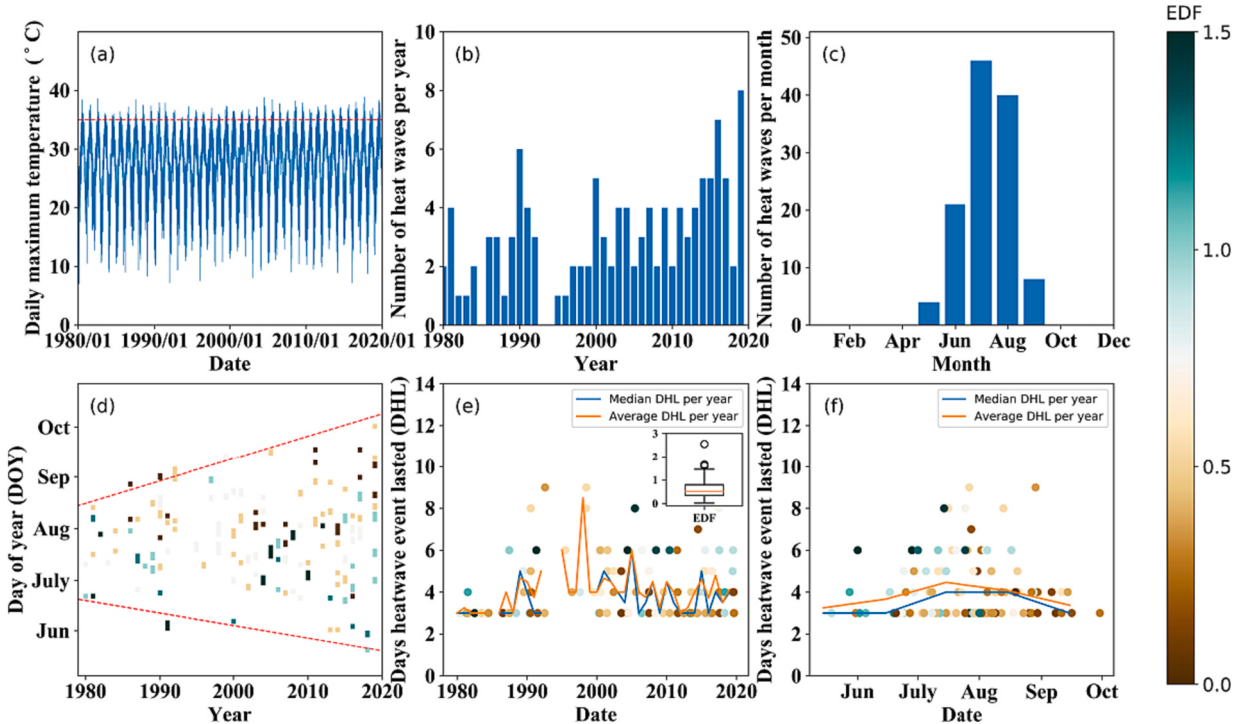


**Fig. 3.** The heatwave related statistics for Shenzhen from 1980 to 2019 include: (a) Daily maximum temperature, (b) Number of heatwave events per year, (c) Number of heatwave events per month, (d) All Heatwaves, (e) Duration of each heatwave, (f) Annual distribution of heatwave duration.

duration of unusual heatwave events significantly increased in recent years. For example, a heatwave event with a duration of nine days occurred on April 1, 2018.

### 3.2. Energy balance analysis from 30 days before to the end of the heatwave

**Fig. 4** displays scatter plots of the daily average energy components 30 days prior to and during 119 heatwave events. Each point on the scatter plot represents a comparison of energy components before and during the heatwave event. In fact, if a heatwave does not occur, the energy before and during the heatwave should change minimally, and all data points are expected to cluster around the  $y = x$  line. The impact of a heatwave on a specific surface is greater when there is increased dispersion in the scatter plot of that surface. We employ the coefficient of variation ( $C_v$ ) to quantify the dispersion of data points in the scatter plot, which also signifies the extent of the heatwave's impact on a city surface. A higher value indicates a greater influence of the heatwave on that surface. The  $C_v$  value in **Fig. 4** (b) is 0.07. This suggests that vegetation is the least affected by heatwaves among the four types of urban surfaces. The reduction in  $LE_{veg}$  during the heatwave is likely due to the combined constraints of water availability and stomatal conductivity in  $LE_{veg}$  (Lobell et al., 2008; Zhou et al., 2021).

Latent heat flux on water surface ( $LE_{water}$ ) represent the process of water diffusion from a water body into the atmosphere. In fact, 53% of the heatwaves have higher  $LE_{water}$  during the heatwave than before the heatwave (see **Fig. 4c**). The coefficient of variation ( $C_v$ ) value in **Fig. 4(c)** is 0.32, which is the largest among **Fig. 4(a-e)**. These results suggest that  $LE_{water}$  significantly changes during the heatwave, which could be attributed to the fact that  $LE_{water}$  is mainly controlled by meteorological elements. Although the latent heat of impervious surfaces ( $LE_{urban}$ ) is relatively smaller among the four land uses (**Figs. 4d** and **5d**), impervious surfaces exert a substantial influence on the urban thermal environment (Chen et al., 2022).

Sensible heat flux refers to the transfer of heat between the surface of the Earth and the atmosphere through conduction and convection. **Fig. 5** (f-j) indicates the increase in the sensible heat flux at various urban surfaces during the heatwave events. Water body usually has a relatively higher specific heat, heatwaves cause little change in the sensible heat flux of the water body. In contrast, the specific heat of impervious surfaces is much lower than that of water bodies, resulting in a higher degree of sensitivity to heatwave-induced changes in sensible heat flux. Specifically, 99% of the scatters in **Fig. 4i** is located on the left side of the 1:1 line. This signifies that in 99% of heatwave events, the average  $H_{urban}$  during the heatwave is higher than the average  $H_{urban}$  30 days before the heatwave. The  $C_v$  value is 0.4, which is the largest among the four types of surfaces. This confirms that impervious surfaces are more susceptible to

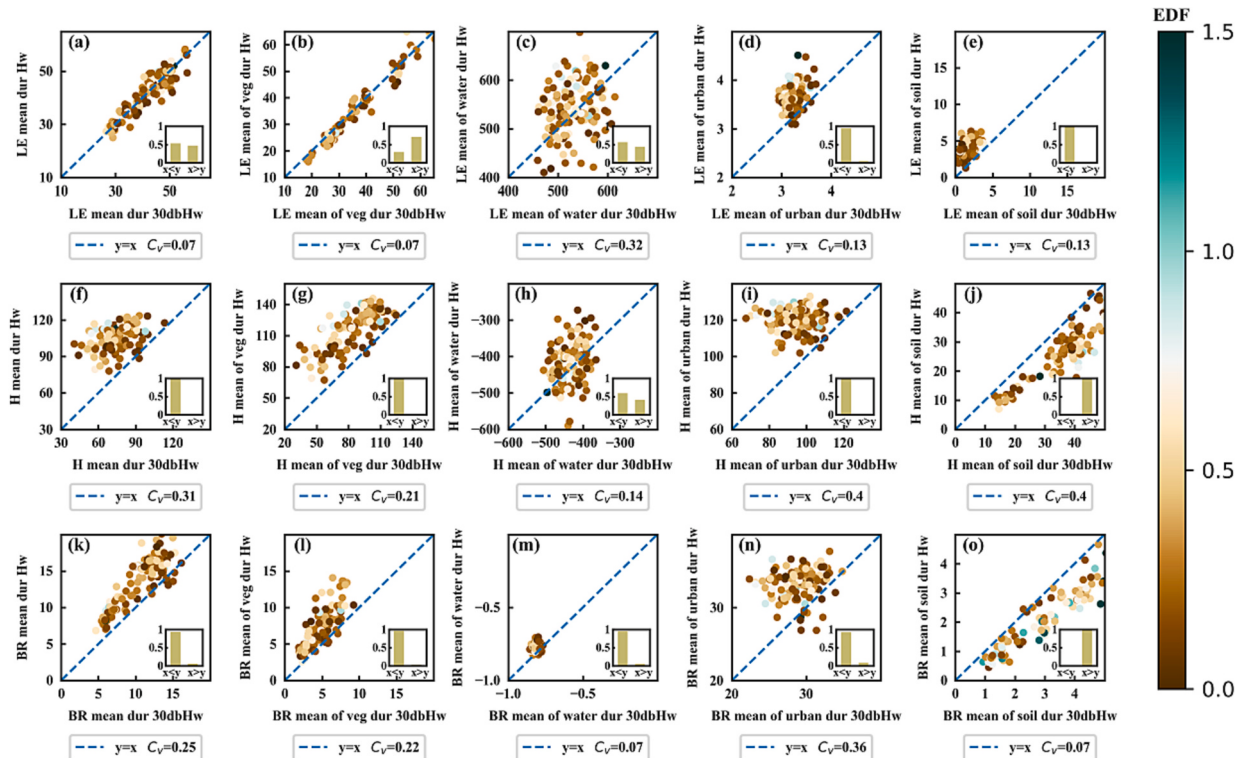


**Fig. 4.** The scatter plots compare the mean values during the 30 days before the heatwave (dur 30dbHw) to the mean values during the heatwave (dur Hw). Each data point in the scatter plot represents an individual heatwave event. LE is the latent heat flux, H is the sensible heat flux, and BR is the Bowen ratio. (a, LE mean; b, LE mean of vegetation; c, LE mean of water; d, LE mean of urban; e, LE mean of soil; f, H mean; g, H mean of vegetation; h, H mean of water; i, H mean of urban; j, H mean of soil; k, BR mean; l, BR mean of vegetation; m, BR mean of water; n, BR mean of urban; o, BR mean of soil).

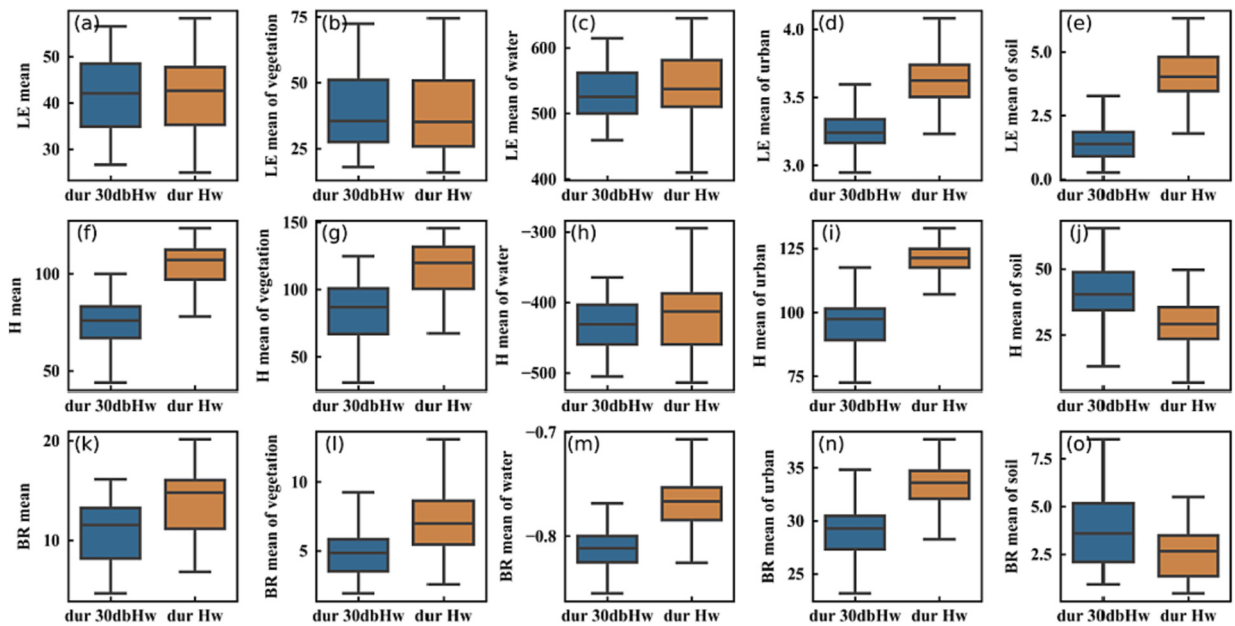


**Fig. 5.** Box plot of the mean of the energy components during the 30 days before (dur 30dbHw) the heatwave compared to the mean during the heatwave(dur Hw) (a, LE mean; b, LE mean of vegetation; c, LE mean of water; d, LE mean of urban; e, LE mean of soil; f, H mean; g, H mean of vegetation; h, H mean of water; i, H mean of urban; j, H mean of soil; k, BR mean; l, BR mean of vegetation; m, BR mean of water; n, BR mean of urban; o, BR mean of soil).

heatwaves, resulting in a larger fluctuation in sensible heat flux change. For water bodies, 54% of the scatters are located on the left side of the 1:1 line according to Fig. 4h. This signifies that in 54% of heatwave events, the average  $H_{water}$  during the heatwave is higher than the average  $H_{water}$  30 days before the heatwave. The  $C_v$  value is 0.14, which is the smallest among the four types of surfaces. This suggests that the sensible heat flux in the water body is less affected by heatwaves. The Bowen ratio is smallest on water surfaces and largest on impervious surfaces among the four urban surface types.

Figs. 6 and 7 shows the spatial distributions of difference in sensible and latent heat fluxes during the heatwave and 30 days before the heatwave for 6 typical heatwave events. Heatwaves in Shenzhen are classified into three categories based on EDF distributions:

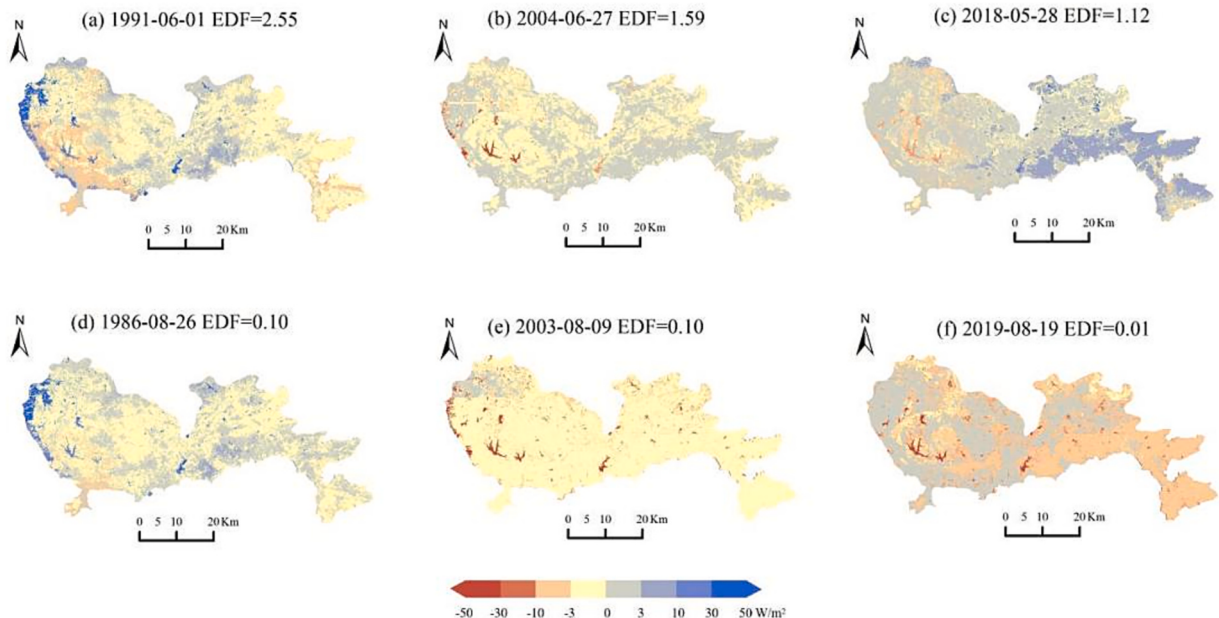


**Fig. 6.** Difference between the mean latent heat fluxes during the heatwave and 30 days before the heatwave in 6 typical heatwave events.

mild discomfort intensity, moderate discomfort intensity, and high discomfort intensity based on EDF distributions (EDF lower than 0.17 at the 10th percentile represent mild-intensity, EDF larger than 1.09 at the 90th percentile represent high-intensity, and EDF larger than 0.17 but lower than 1.09 represent moderate-intensity). One high-intensity and one low-intensity heatwave event are selected for each period around 1980, 2000 and 2019, consequence a total of 6 typical heatwave events are selected. The selected years, 1980, 2000, and 2019, represent different urban imperviousness rates, reflecting distinct levels of urbanization in Shenzhen (Fig. 1). Compared to other urban areas, the energy changes in water surface before and during heatwaves exhibit noticeable distinctions (Figs. 6 and 7). Furthermore, the energy variations to the east of Shenzhen before and during heatwave events are more pronounced than those to the west, possibly due to the proximity to the sea on the eastern side (Figs. 6 and 7). As the current time approaches, there is an observable escalation in energy changes both before and during heatwaves throughout the entire region (Figs. 6 and 7), possibly associated with a rise in impermeable surfaces within the city (Mohammadi and Taylor, 2017).

### 3.3. Effects of energy changes before and during the heatwave on human comfort

Fig. 8 shows the relationship between the difference in average energy components (EC) during the heatwave and 30 days prior ( $\Delta EC$ ) and human comfort (EDF). The calculation method for  $\Delta EC$  is detailed in Eqs. (9)–(11). The data types are normalized, and the scatter plot has been linearly fitted. The slope of the linear fit ( $K$ ) represents the effect of  $\Delta EC$  on human comfort (EDF) during the heatwave for various urban surfaces. A larger  $K$  value indicates a more significant impact of the  $\Delta EC$  on human comfort during the heatwave. Consequently, the slope of the linear fit between the  $\Delta EC$  and human comfort during the heatwave serves as an indicator of the surface's regulatory capacity in sustaining human comfort under such circumstances. In 2019, Shenzhen's urban imperviousness (UI) is 39.14% (see Fig. 1). The scatter points on the plot have been divided into two categories based on different UI values (0–0.2 and 0.2–0.4). The scatter points for different UI values are independently fitted to investigate the effect of  $\Delta EC$  on human comfort under different UI conditions.

Both vegetation and water surfaces have a significant impact on the water cycle of terrestrial ecosystems. The physiological regulation of vegetation and the high heat capacity of water bodies reduce the impact of urban heat islands and heatwaves on human comfort through evaporative cooling effects (Steneveld et al., 2014). Therefore, a larger  $K$  value represents a more significant impact of the  $\Delta LE$  on the EDF during the heatwave. In other words, it indicates a reduced capacity of the urban surface to regulate human comfort. The vegetation's  $K$  value is 0.43 (see Fig. 8b), which is smaller compared to water surfaces. This indicates that the changes in EDF caused by  $\Delta LE$  on the vegetation surface are smaller than those on water surfaces. These findings confirm that vegetation surfaces possess a greater capacity to regulate human comfort compared to water surfaces.

Analyzing the  $K$  for  $\Delta LE$  in the water body (Fig. 8c) is important since a higher  $\Delta LE$  in the water body results in a larger EDF and a higher degree of discomfort.  $\Delta LE$  of the water body is primarily influenced by surface meteorological factors. Higher temperatures and radiation during heatwaves lead to a larger  $LE_{water}$ , which accelerates the transfer of natural water surfaces to atmospheric water, thereby increasing the relative humidity and EDF during heatwaves. However, a higher  $LE_{water}$  lead to a smaller  $H_{water}$ , which decreases the EDF during heatwave events. In general, a greater  $\Delta LE$  in the water body causes a larger EDF and a higher degree of

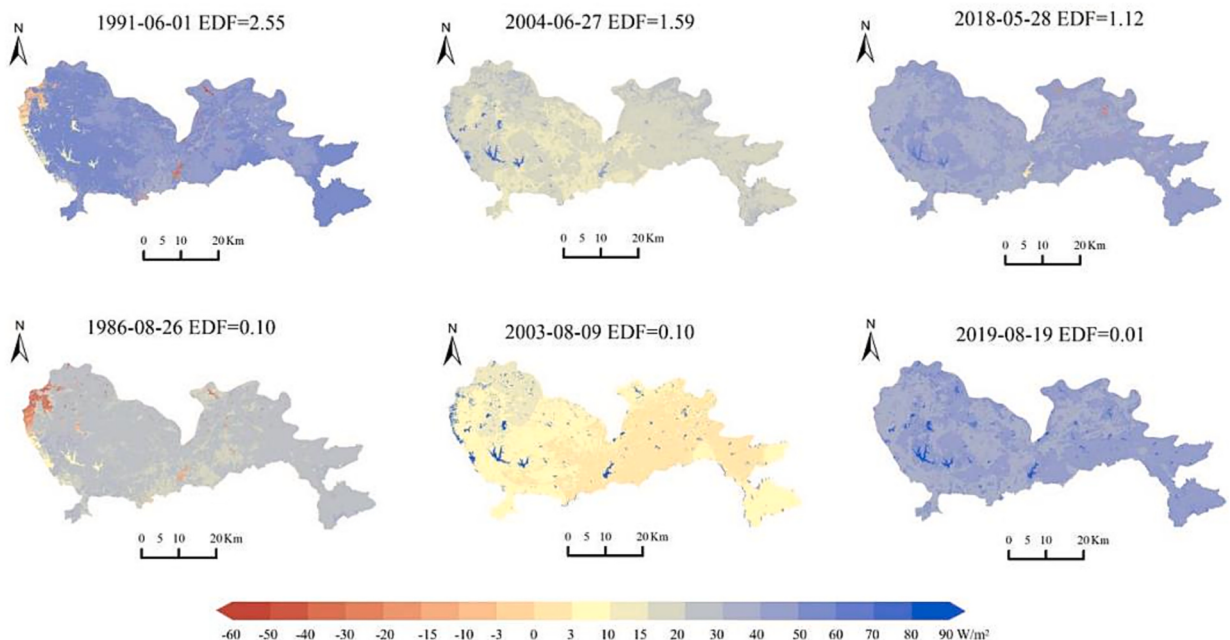


**Fig. 7.** Difference between the mean sensible heat fluxes during the heatwave and 30 days before the heatwave in 6 typical heatwave events.

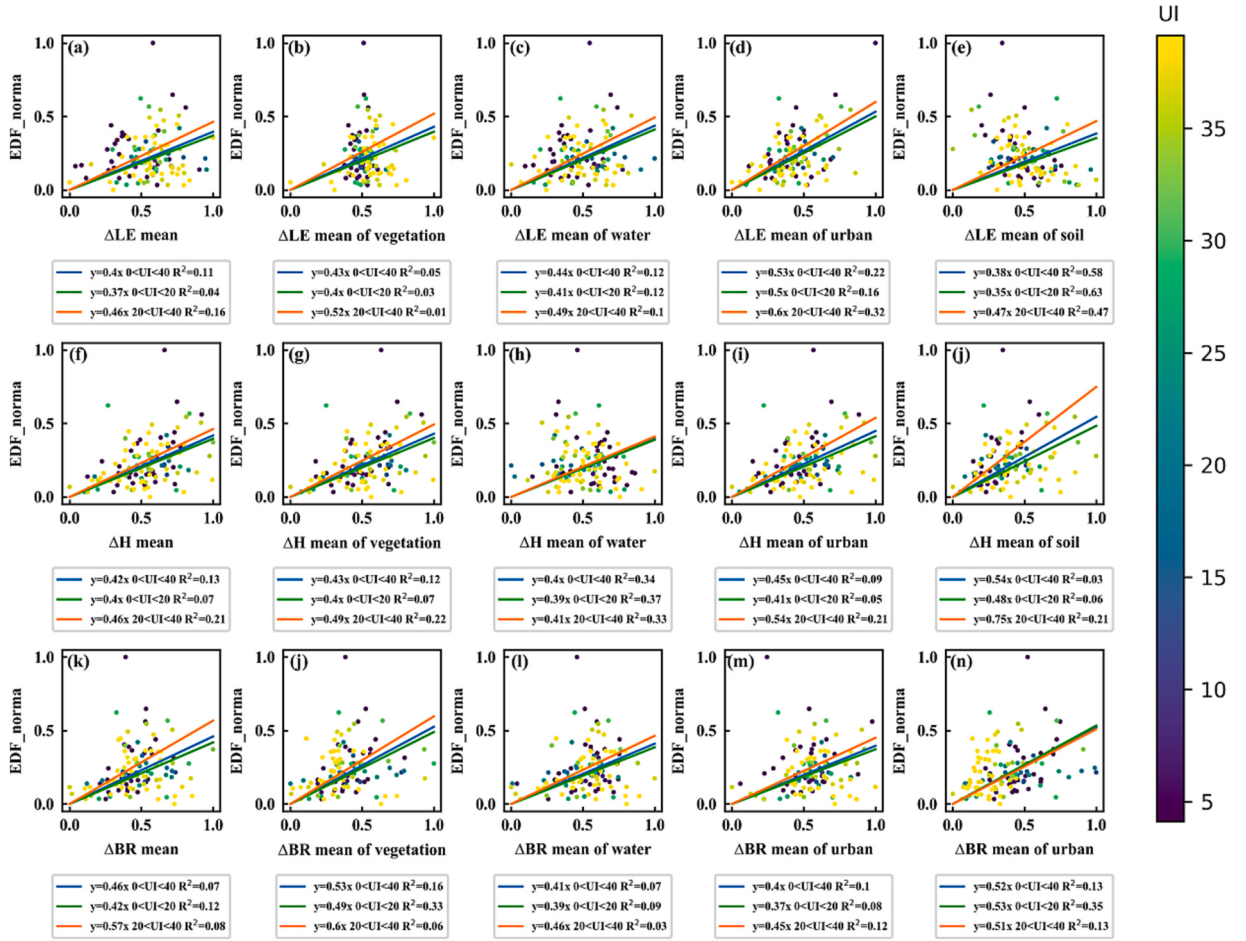


**Fig. 8.** The relationship between the difference in average energy components (EC) during the heatwave and 30 days prior ( $\Delta EC$ ) (a,  $\Delta LE$  mean; b,  $\Delta LE$  mean of vegetation; c,  $\Delta LE$  mean of water; d,  $\Delta LE$  mean of urban; e,  $\Delta LE$  mean of soil; f,  $\Delta H$  mean; g,  $\Delta H$  mean of vegetation; h,  $\Delta H$  mean of water; i,  $\Delta H$  mean of urban; j,  $\Delta H$  mean of soil; k,  $\Delta BR$  mean; l,  $\Delta BR$  mean of vegetation; m,  $\Delta BR$  mean of water; n,  $\Delta BR$  mean of urban; o,  $\Delta BR$  mean of soil) and human comfort (EDF). The UI represents the urban imperiousness.

discomfort. Additionally, the water body has a weaker ability to regulate regional human comfort compared to vegetation surfaces.

The  $\Delta LE$  in urban areas causes the most significant alteration in EDF and has the greatest impact on human comfort. As per Eq. (6),  $LE_{urban}$  is primarily influenced by air temperature, vapor pressure deficit, and wind speed. Meanwhile, EDF is determined by relative humidity and air temperature. The factors that affect  $\Delta LE$  in urban areas and EDF are quite similar, which leads to the  $\Delta LE$  in urban areas being the most significant factor in influencing EDF.

The fitting coefficients for the vegetation  $\Delta LE$  and EDF are 0.4 and 0.52 under UI of 0–0.2 and 0.2–0.4, respectively, (Fig. 8b). These results suggest that urbanization exacerbates the effect of vegetation  $\Delta LE$  on the EDF during heatwaves. In other words, urbanization reduced the ability of vegetation to regulate heatwave and human comfort. This can be explained as the increased urban heat island effect caused by urbanization and the high frequent extreme temperatures occurrence during heatwaves caused by climate change in recent years (Ramamurthy et al., 2016; Perkins-Kirkpatrick and Lewis, 2020).

The fitting coefficients for the  $\Delta H$  and EDF during the heatwave are 0.43, 0.4, 0.45, and 0.54, for vegetation, water surface, impervious, and soil surfaces, respectively (Fig. 8g-j). The fitting coefficient is 0.43 for vegetation surface, indicate that a larger vegetation  $\Delta H$  lead to a higher EDF and a lower comfort. The larger vegetation  $\Delta H$  can be attributed to the higher temperature during the heatwave, which inhibit stomatal conductivity and weaken the vegetation's ability to regulate thermal environment.

The fit coefficient between the  $\Delta H$  in water body and the EDF during the heatwave is 0.4 (Fig. 8h). This indicates that a larger  $\Delta H$  in the water body results in a higher EDF and a lower level of human comfort during the heatwave. The impervious surface has the highest K value between urban  $\Delta H$  and EDF, indicating that the  $\Delta H$  in the impervious surface has the greatest impact on EDF. The impervious surface experiences a sharp increase in temperature during a heatwave due to its lower specific heat capacity, resulting in significant changes in surface temperature and sensible heat flux. Therefore, the  $\Delta H$  in impervious surface is the most accurate indicator of discomfort degree in Shenzhen during the heatwave events.

The fitted straight lines K between the  $\Delta H$  in impervious surface and EDF are 0.41 and 0.54 under the UI of 0–0.2 and 0.2–0.4,

respectively (Fig. 8i). A higher urban imperviousness value under the same  $\Delta H$  will lead to a higher EDF and a lower comfort level. This effect could be attributed to the urbanization process exacerbates the urban heatwave effect. The fitting coefficients for the vegetation  $\Delta H$  and EDF during heatwaves are 0.4 and 0.49 under the UI of 0–0.2 and 0.2–0.4, respectively (Fig. 8g). The urbanization process has increased the effect of the vegetation  $\Delta H$  on EDF by 22.5%. Therefore, urbanization has reduced the capacity of vegetation to regulate human comfort during the heatwaves by 22.5% in 40 years. Moreover, for every 1% increase in urbanization rate, the regulating capacity of vegetation for human comfort decreases by 0.64%. With urbanization, the same  $\Delta H$  results in higher EDF and lower comfort levels. Both patterns of latent heat flux and sensible heat flux suggest that the mitigation capacity of vegetation on the human comfort level decreases with urbanization.

## 4. Discussion

### 4.1. Urban resilience to heatwaves

The urban underlying surface is inherently intricate, and meteorological data often fall short in capturing nuanced variations on urban surfaces. However, by integrating high-resolution reflectance data from satellite imagery and urban remote sensing energy model, it becomes possible to quantify fine-grained changes on the urban surface at a high resolution (Chen et al., 2022). This is the rationale behind considering urban surface energy, rather than relying solely on meteorological data, to characterize the impact of heatwaves in this study.

Indeed, this study introduces novel considerations for assessing the impact of heatwaves on cities and different urban surfaces, as well as evaluating urban resilience during heatwave events. While cities themselves lack life, the individuals within them possess the capacity to perceive temperature variations. Urban resilience, in this context, is contemplated through four fundamental pillars: resisting, recovering, adapting and transforming (Qing et al., 2023). This study establishes a relationship between changes in energy before and during heatwave events and human thermal comfort during heatwaves. This relationship is employed to assess the adaptability and recovery of the entire urban area, as well as different urban surfaces, to heatwaves. If there is a significant change in energy for a specific urban surface before and during a heatwave, indicating substantial heatwave intensity, yet human thermal comfort during the heatwave is notably high, it suggests that this surface possesses elevated resistance and adaptation capabilities to the heatwave. In essence, this urban surface demonstrates increased resilience to heatwaves.

### 4.2. The impact of urbanization on vegetation's capacity to regulate human comfort during heatwaves

The discomfort index is particularly useful in regions with high temperatures and humidity, such as tropical and subtropical areas (Liu et al., 2019). Shenzhen is a coastal city with a humid and warm climate. The discomfort index is very suitable for evaluating the human comfort level in Shenzhen during heatwaves. As indicated by Eq. (4), vegetation plays a crucial role in regulating human comfort by controlling humidity and temperature. Urbanization degrades the ability of vegetation to regulate human comfort during heatwaves, due to the following reasons:

1. Temperature rise have a significant impact on vegetation, affecting its optical properties such as chlorophyll content, light absorption, and reflectance, which can inhibit plant growth and reduce NDVI (Rastogi et al., 2020). Extreme high temperatures also damage plant cell walls, membranes, and proteins (Bita and Gerats, 2013). In recent years, high frequency heatwaves and extreme climates have caused vegetation growth stagnation and even death (Allen et al., 2010). These adverse factors can reduce vegetation's ability to regulate human comfort during heatwaves.
2. The height of forest vegetation is relatively higher (usually higher than 10 m), therefore its temperature regulation function is relatively stronger. Meanwhile, forests can provide shade, shelter, and obstruct direct sunlight on the ground surface, which further reduces surface temperature (Bonan, 2008). In addition, the density of forest vegetation is relatively higher, which can intercept more rainwater and retain moisture (Liu et al., 2018). Overall, the ability of forests to regulate human comfort is stronger than that of grasslands. The urbanization process has led to a decrease in the proportion of grasslands and forests, resulting in a reduced ability of vegetation to regulate human comfort.
3. Vegetation can provide shade for the impermeable surface, reducing the amount of heat absorbed by them and helping to regulate the ambient temperature (Yu and Hien, 2006; Taleghani et al., 2015). With urbanization progress, buildings become taller, and green spaces are constructed (Escobedo et al., 2011). As a result, large areas of vegetation are replaced by scattered urban greenery, reducing the capacity of vegetation to provide shade for impermeable surfaces.

### 4.3. Primary sources of uncertainty

#### (1) Uncertainty from EDF parameters

The discomfort index is used in this study to measure human discomfort. Nevertheless, the wet bulb globe temperature (WBGT) is the most widely used heat stress index. The WBGT is recommended by many international organizations for exposing workers in hot environments and has been selected as an International Organization for Standardization (ISO) standard (Parsons, 2006). The WBGT is calculated as follows:

$$WBGT = 0.7T_w + 0.2T_g + 0.1T_a \quad (12)$$

where  $T_w$  represent wet bulb temperature,  $T_g$  represent black globe temperature and  $T_a$  represent ambient temperature (Lemke and Kjellstrom, 2012). However, the inherent limitation of the WBGT is that its applicability requires measuring  $T_g$ , which is difficult to obtain. The  $T_g$  is measured using a temperature sensor placed in the center of a thin copper black sphere (diameter: 150 mm), and it needs to be corrected for different clothing (e.g., protective clothing) and different metabolic rates. Therefore, WBGT has inevitable uncertainties and limitations when assessing heat stress over a long time series in a specific study region. We evaluated four indicators associated with the WBGT index: the Oxford index (WD), Discomfort index (DI), Fighter index of thermal stress (FITS), and Modified discomfort index (MDI). All these indices demonstrate a strong correlation with the WBGT, with  $R^2$  values ranging from 0.930 to 0.967. Notably, the Discomfort Index (DI) stands as the only index, aside from the WBGT, that has been employed for over four decades. This index estimates thermal comfort by combining relative humidity and temperature, rendering it particularly suitable for regions characterized by high temperatures and humidity, such as Shenzhen. The DI values are very close to the WBGT index with an  $R^2$  value of 0.9466 between DI and WBGT ( $R^2 = 0.999$ ; SE = 0.0035) (Epstein and Moran, 2006).

#### (2) Uncertainty from input data set.

ERA5 uses a weather forecasting model to generate a continuous spatial and temporal dataset. However, the generated dataset contains certain uncertainty, which can result in biased energy component estimates. In addition, extracting urban land use from Landsat imagery can also lead to errors, which will be accumulated into the model output.

#### (3) Uncertainty from the urban four-source model

The performance of the FSU model has been validated by Chen et al. (2022) at two EC sites in the main urban and suburbs of Tianjin. The model has also been used to reconstruct urban ET in Tianjin from 1986 to 2021. However, there are uncertainties involved in the model mechanism, assumptions and selection of model parameters. Firstly, the FSU model adopt the ‘patch’ and ‘layers’ mechanisms, assuming that the energy balance of different urban surfaces does not exchange with each other. However, the water vapor and energy exchange occurs on all types of urban surfaces due to the advection effect (Chen et al., 2023a, 2023b). Second, previous studies have proved that the uncertainty of sensible and latent heat fluxes calculations mainly comes from the determinations of aerodynamic impedance and surface impedance parameters (Chen et al., 2022). For example,  $Z_{om}$  requires the inputs of vegetation height and building height, which lead to large uncertainty.

#### (4) Uncertainty from the urban soil surface

The fitting results of the soil surface in Fig. 8 may entail uncertainties. In this study, the energy difference before and during the heatwaves in different urban surface represents the average for the respective urban surface areas. Considering the potential misclassification of soil surfaces in land-use classifications, especially when compared to vegetation, water surfaces, and impermeable surfaces, there is a relatively high likelihood of misclassification for soil surfaces (Kuras et al., 2021). Additionally, the proportion of soil surfaces in urban areas is relatively small (Fig. 9). Consequently, there is substantial uncertainty in the fitting results for soil surfaces. Vegetation, impermeable surfaces, and water surfaces constitute the majority of urban land cover, as illustrated in the figure below, with soil accounting for only 0.02–0.06%. The overall regulatory capacity of soil in mitigating heatwaves is limited, and its impact can be disregarded.

## 5. Conclusions

In this study, we used a stomatal process-based urban energy balance model (SUE model) to reconstruct the daily energy components before and during heatwave events in Shenzhen, China. The Excess Discomfort Factor (EDF) provides an indicator of the level of human comfort experienced during a heatwave, which is calculated by combining the Discomfort Index (DI) and the Excess Heat Factor (EHF). We investigated the impacts of heatwaves on various urban surfaces and revealed the regulatory mechanisms of different urban surfaces on human comfort. During the heatwave, while vegetation was found to have a stronger ability to regulate human

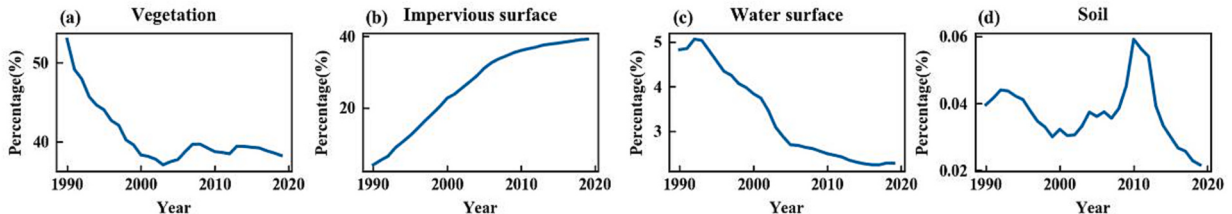


**Fig. 9.** The changes in the proportions of (a) vegetation surface, (b) impermeable surface, (c) water surface, and (d) soil surface in Shenzhen from 1990 to 2019.

comfort compared to water surfaces, urbanization has diminished this capacity by 22.5% in recent years. Interestingly, we found that energy changes in impervious surfaces during heatwaves showed the strongest correlation with human comfort levels. Therefore, tracking energy changes in impervious surfaces can provide the most accurate reflection of human comfort during heatwaves.

#### CRediT authorship contribution statement

**Yizhao Wei:** Writing – review & editing, Writing – original draft, Visualization, Validation, Software, Methodology, Investigation, Formal analysis, Data curation, Conceptualization. **Han Chen:** Writing – review & editing, Supervision, Resources, Project administration, Funding acquisition, Conceptualization. **Jinhui Jeanne Huang:** Writing – review & editing, Supervision, Resources, Project administration, Investigation, Funding acquisition, Conceptualization.

#### Declaration of competing interest

The authors declare that they have no known competing financial interests or personal relationships that could have appeared to influence the work reported in this paper.

#### Data availability

Data will be made available on request.

#### Acknowledgements

The authors acknowledge the financial support from the National Key Research and Development Program under the grant number No.-2022YFF1301101, Shenzhen Ecological and Environmental Monitoring Center Station Program under the grant number 20230601, Shenzhen Science and Technology Program under the grant number JCY20210324120807021, National Natural Science Foundation of China under the grant number 42101033 and National Key Research and Development Program of China under the grant number 2021YFC3200400. We thank the anonymous reviewers for their valuable suggestions that allowed us to improve the paper.

#### Appendix A

$r_{ah}$  is the aerodynamic resistance in s/m. It is calculated using the following expression:

$$r_{ah} = \frac{\left[ \ln\left(\frac{z_u - d_0}{z_{0M}}\right) - \psi_M \right] \left[ \ln\left(\frac{z_t - d_0}{z_{0H}}\right) - \psi_H \right]}{k^2 u} \quad (13)$$

where  $z_u$  and  $z_t$  are the respective heights, in m/s, at which the wind speed  $u$  and atmospheric temperature are measured,  $d_0$  is the displacement height, and  $z_{0M}$  and  $z_{0H}$  are the roughness lengths for momentum and heat transport, respectively. All measurements are in meters. In addition,  $\psi_M$  and  $\psi_H$  are stability correction functions for momentum and heat, which depend on the Monin-Obukhov length (Brutsaert, 2013), and  $k$  is von Karman's constant ( $= 0.4$ ).

$$\lambda = (2.501 - 0.0024T) \times 10^6 \quad (14)$$

$$\Delta = \frac{4098 \left[ 0.6108 \exp\left(\frac{17.27T}{(T+237.3)}\right) \right]}{(T + 237.3)^2} \times 10^3 \quad (15)$$

$$\gamma = \frac{C_p P_a}{\mu \lambda} \quad (16)$$

$T$  is the temperature (K). The specific heat of air at constant pressure  $C_p$  takes the value of 1013 (J/kg/K),  $P_a$  is the atmospheric pressure (Pa),  $\mu$  is the molecular weight ratio of water vapor to dry air,  $\mu = 0.622$ .  $\gamma$  is psychrometric constant.  $\Delta$  represents the vapor pressure difference (hpa).

#### References

- Ahmed, I., van Esch, M., van der Hoeven, F., 2023. Heatwave vulnerability across different spatial scales: insights from the dutch built environment. *Urban Clim.* 51, 101614 <https://doi.org/10.1016/j.jclim.2023.101614>.
- Allen, C.D., Macalady, A.K., Chenchouini, H., Bachelet, D., McDowell, N., Vennetier, M., Kitzberger, T., et al., 2010. A global overview of drought and heat-induced tree mortality reveals emerging climate change risks for forests. *For. Ecol. Manag.* 259 (4), 660–684. <https://doi.org/10.1016/j.foreco.2009.09.001>.

- Barriopedro, D., Fischer, E.M., Luterbacher, J.U.R., Trigo, R.M., R. Garc I A-Herrera., 2011. The hot summer of 2010: redrawing the temperature record map of europe. *Science* 332 (6026), 220–224. <https://doi.org/10.1126/science.1201224>.
- Becker, S., Potchter, O., Yaakov, Y., 2003. Calculated and observed human thermal sensation in an extremely hot and dry climate. *Energ. Build.* 35 (8), 747–756. [https://doi.org/10.1016/S0378-7788\(02\)00228-1](https://doi.org/10.1016/S0378-7788(02)00228-1).
- Bita, C.E., Gerats, T., 2013. Plant tolerance to high temperature in a changing environment: scientific fundamentals and production of heat stress-tolerant crops. *Front. Plant Sci.* 4, 273. <https://doi.org/10.3389/fpls.2013.00273>.
- Bonan, G.B., 2008. Forests and climate change: forcings, feedbacks, and the climate benefits of forests. *Science* 320 (5882), 1444–1449. <https://doi.org/10.1126/science.1155121>.
- Brutsaert, W., 2013. *Evaporation into the Atmosphere: Theory, History and Applications*. Springer Science \& Business Media.
- Chen, H., Huang, J.J., Dash, S.S., Mcbean, E., Wei, Y., Li, H., 2022. Assessing the impact of urbanization on urban evapotranspiration and its components using a novel four-source energy balance model. *Agric. For. Meteorol.* 316, 108853 <https://doi.org/10.1016/j.agrmet.2022.108853>.
- Chen, H., Huang, J.J., Liang, H., Wang, W., Li, H., Wei, Y., Jiang, A.Z., Zhang, P., 2023a. Integration of flux footprint and physical mechanism into convolutional neural network model for enhanced simulation of urban evapotranspiration. *J. Hydrol.* 619, 129016 <https://doi.org/10.1016/j.jhydrol.2022.129016>.
- Chen, H., Huang, J.J., Liang, H., Wang, W., Li, H., Wei, Y., Jiang, A.Z., Zhang, P., 2023b. Can evaporation from urban impervious surfaces be ignored? *J. Hydrol.* 616, 128582 <https://doi.org/10.1016/j.jhydrol.2022.128582>.
- Chew, L.W., Liu, X., Li, X., Norford, L.K., 2021. Interaction between heat wave and urban heat island: a case study in a tropical coastal city, Singapore. *Atmos. Res.* 247, 105134 <https://doi.org/10.1016/j.atmosres.2020.105134>.
- Conti, S., Masocco, M., Meli, P., Minelli, G., Palummeri, E., Solimini, R., Toccaceli, V., Vichi, M., 2007. General and specific mortality among the elderly during the 2003 heat wave in genoa (Italy). *Environ. Res.* 103 (2), 267–274. <https://doi.org/10.1016/j.envres.2006.06.003>.
- Da Silva, V.D.P.R., de Azevedo, P.V., Brito, R.S., Da Cunha Campos, J.A.O.H., 2010. Evaluating the urban climate of a typically tropical city of northeastern Brazil. *Environ. Monit. Assess.* 161 (1), 45–59. <https://doi.org/10.1007/s10661-008-0726-3>.
- Di Bernardino, A., Falasca, S., Iannarelli, A.M., Casadio, S., Siani, A.M., 2023. Effect of heatwaves on urban sea breeze, heat island intensity, and outdoor thermo-hygrometric comfort in Rome (Italy). *Urban Clim.* 52, 101735 <https://doi.org/10.1016/j.ulclim.2023.101735>.
- Epstein, Y., Moran, D.S., 2006. Thermal comfort and the heat stress indices. *Ind. Health* 44 (3), 388–398. <https://doi.org/10.2486/indhealth.44.388>.
- Escobedo, F.J., Kroeger, T., Wagner, J.E., 2011. Urban forests and pollution mitigation: analyzing ecosystem services and disservices. *Environ. Pollut.* 159 (8–9), 2078–2087. <https://doi.org/10.1016/j.envpol.2011.01.010>.
- Garc I A-Herrera, R., Az, J.E.D.I., Trigo, R.M., Luterbacher, J.U.R., Fischer, E.M., 2010. A review of the european summer heat wave of 2003. *Crit. Rev. Environ. Sci. Technol.* 40 (4), 267–306. <https://doi.org/10.1080/10643380802238137>.
- Hatvani-Kovacs, G., Belusko, M., Pockett, J., Boland, J., 2016. Can the excess heat factor indicate heatwave-related morbidity? A case study in Adelaide, South Australia. *Ecohealth* 13 (1), 100–110. <https://doi.org/10.1007/s10393-015-1085-5>.
- He, B., 2023. Cause-related injustice, process-related injustice, effect-related injustice and regional heat action planning priorities: an empirical study in yangtze river delta and Chengdu-Chongqing urban agglomerations. *Lands. Urban Plan.* 237, 104800 <https://doi.org/10.1016/j.landurbplan.2023.104800>.
- He, B., Ding, L., Prasad, D., 2020a. Relationships among local-scale urban morphology, urban ventilation, urban heat island and outdoor thermal comfort under sea breeze influence. *Sustain. Cities Soc.* 60, 102289 <https://doi.org/10.1016/j.scs.2020.102289>.
- He, X., Wang, J., Feng, J., Yan, Z., Miao, S., Zhang, Y., Xia, J., 2020b. Observational and modeling study of interactions between urban heat island and heatwave in Beijing. *J. Clean. Prod.* 247, 119169 <https://doi.org/10.1016/j.jclepro.2019.119169>.
- He, B., Wang, J., Zhu, J., Qi, J., 2022. Beating the urban heat: situation, background, impacts and the way forward in China. *Renew. Sust. Energ. Rev.* 161, 112350 <https://doi.org/10.1016/j.rser.2022.112350>.
- Hersbach, H., Bell, B., Berrisford, P., Hirahara, S., Nyi, A.A.S. Hor A., Mu, J.I.N., Oz-Sabater, N., Nicolas, J., et al., 2020. The era5 global reanalysis. *Q. J. R. Meteorol. Soc.* 146 (730), 1999–2049.
- Huang, Y., Song, H., Cheng, Y., Bi, P., Li, Y., Yao, X., 2023a. Heatwave and urinary hospital admissions in China: disease burden and associated economic loss, 2014 to 2019. *Sci. Total Environ.* 857, 159565 <https://doi.org/10.1016/j.scitotenv.2022.159565>.
- Huang, X., Yao, R., Xu, T., Zhang, S., 2023b. The impact of heatwaves on human perceived thermal comfort and thermal resilience potential in urban public open spaces. *Build. Environ.* 242, 110586 <https://doi.org/10.1016/j.buildenv.2023.110586>.
- Jiang, S., Lee, X., Wang, J., Wang, K., 2019. Amplified urban heat islands during heat wave periods. *J. Geophys. Res. Atmos.* 124 (14), 7797–7812. <https://doi.org/10.1029/2018JD030230>.
- Jingyi, B., Guojing, G., Jiahao, C., Yanxin, S., Garcia, M., Yanchun, G., 2021. Biophysical constraints on evapotranspiration partitioning for a conductance-based two source energy balance model. *J. Hydrol.* (Amst.) 603, 127179. <https://doi.org/10.1016/j.jhydrol.2021.127179>.
- Jung, W., Jazizadeh, F., Diller, T.E., 2019. Heat flux sensing for machine-learning-based personal thermal comfort modeling. *Sensors* 19 (17). <https://doi.org/10.3390/s19173691>.
- Kong, J., Zhao, Y., Strelbel, D., Gao, K., Carmeliet, J., Lei, C., 2023. Understanding the impact of heatwave on urban heat in greater Sydney: temporal surface energy budget change with land types. *Sci. Total Environ.* 903, 166374 <https://doi.org/10.1016/j.scitotenv.2023.166374>.
- Kuras, A., Brell, M., Rizzi, J., Burud, I., 2021. Hyperspectral and lidar data applied to the urban land cover machine learning and neural-network-based classification: a review. *Remote Sens.* 13 (17), 3393.
- Langlois, N., Herbst, J., Mason, K., Nairn, J., Byard, R.W., 2013. Using the excess heat factor (ehf) to predict the risk of heat related deaths. *J. Forensic Legal Med.* 20 (5), 408–411. <https://doi.org/10.1016/j.jflm.2012.12.005>.
- Lemke, B., Kjellstrom, T., 2012. Calculating workplace wbgt from meteorological data: a tool for climate change assessment. *Ind. Health* 50 (4), 267–278. <https://doi.org/10.2486/indhealth.MS1352>.
- Lhomme, J.P., Montes, C., Jacob, F., Prévôt, L., 2012. Evaporation from heterogeneous and sparse canopies: on the formulations related to multi-source representations. *Bound.-Layer Meteorol.* 144 (2), 243–262. <https://doi.org/10.1007/s10546-012-9713-x>.
- Li, N., Zhang, Y., Zhang, Y., Shi, K., Qian, H., Yang, H., Niu, Y., et al., 2023. The unprecedented 2022 extreme summer heatwaves increased harmful cyanobacteria blooms. *Sci. Total Environ.* 896, 165312 <https://doi.org/10.1016/j.scitotenv.2023.165312>.
- Liang, L., Yu, L., Wang, Z., 2022. Identifying the dominant impact factors and their contributions to heatwave events over mainland China. *Sci. Total Environ.* 848, 157527 <https://doi.org/10.1016/j.scitotenv.2022.157527>.
- Liu, H., Zhang, M., Lin, Z., Xu, X., 2018. Spatial heterogeneity of the relationship between vegetation dynamics and climate change and their driving forces at multiple time scales in Southwest China. *Agric. For. Meteorol.* 256, 10–21.
- Liu, X., Li, L., Liu, X., Zhang, T., 2019. Analysis of passenger flow and its influences on hvac systems: an agent based simulation in a chinese hub airport terminal. *Build. Environ.* 154, 55–67. <https://doi.org/10.1016/j.buildenv.2019.03.011>.
- Lobell, D.B., Bonfils, C.J., Kueppers, L.M., Snyder, M.A., 2008. Irrigation cooling effect on temperature and heat index extremes. *Geophys. Res. Lett.* 35 (9) <https://doi.org/10.1029/2008GL034145>.
- Loughran, T.F., Perkins-Kirkpatrick, S.E., Alexander, L.V., 2017. Understanding the spatio-temporal influence of climate variability on australian heatwaves. *Int. J. Climatol.* 37 (10), 3963–3975. <https://doi.org/10.1002/joc.4971>.
- Ma, X., Miao, S., Masson, V., Wurtz, J., Zhang, Y., Wang, J., Huang, X., Yan, C., 2024. The synergistic effects of urbanization and an extreme heatwave event on urban thermal environment in Paris. *Urban Clim.* 53, 101785 <https://doi.org/10.1016/j.ulclim.2023.101785>.
- Mazdiyasi, O., Aghakouchak, A., 2015. Substantial increase in concurrent droughts and heatwaves in the United States. *Proc. Natl. Acad. Sci.* 112 (37), 11484–11489. <https://doi.org/10.1073/pnas.1422945112>.
- Mcmahon, T.A., Peel, M.C., Lowe, L., Srikanthan, R., Mcvicar, T.R., 2013. Estimating actual, potential, reference crop and pan evaporation using standard meteorological data: a pragmatic synthesis. *Hydrol. Earth Syst. Sci.* 17 (4), 1331–1363. <https://doi.org/10.5194/hess-17-1331-2013>.

- Miralles, D.G., Van Den Berg, M.J., Teuling, A.J., De Jeu, R., 2012. Soil moisture-temperature coupling: a multiscale observational analysis. *Geophys. Res. Lett.* 39 (21) <https://doi.org/10.1029/2012GL053703>.
- Miralles, D.G., Teuling, A.J., van Heerwaarden, C.C., Vilà-Guerau De Arellano, J., 2014. Mega-heatwave temperatures due to combined soil desiccation and atmospheric heat accumulation. *Nat. Geosci.* 7 (5), 345–349. <https://doi.org/10.1038/ngeo2141>.
- Mohammadi, N., Taylor, J.E., 2017. Urban energy flux: spatiotemporal fluctuations of building energy consumption and human mobility-driven prediction. *Appl. Energy* 195, 810–818.
- Moreno-Fernandez, J., Sastre, J., Herranz, S., Pinés, P., Gomez, F.J., Quiroga, I., Moya, A.J., et al., 2023. Effect of the historic spanish heatwave over glycemic control in adult patients with type 1 diabetes. *Sci. Total Environ.* 889, 164045 <https://doi.org/10.1016/j.scitotenv.2023.164045>.
- Nairn, J.R., Fawcett, R.J., 2015. The excess heat factor: a metric for heatwave intensity and its use in classifying heatwave severity. *Int. J. Environ. Res. Public Health* 12 (1), 227–235. <https://doi.org/10.3390/ijerph12010027>.
- Parsons, K., 2006. Heat stress standard iso 7243 and its global application. *Ind. Health* 44 (3), 368–379. <https://doi.org/10.2486/indhealth.44.368>.
- Perkins-Kirkpatrick, S.E., Lewis, S.C., 2020. Increasing trends in regional heatwaves. *Nat. Commun.* 11 (1), 1–8. <https://doi.org/10.1038/s41467-020-16970-7>.
- Piticar, A., Croitoru, A.E., Ciupercă, F.A., Harpa, G.V., 2018. Recent changes in heat waves and cold waves detected based on excess heat factor and excess cold factor in Romania. *Int. J. Climatol.* 38 (4), 1777–1793. <https://doi.org/10.1002/joc.5295>.
- Qing, Y., Wang, S., Yang, Z., Gentile, P., 2023. Soil moisture–atmosphere feedbacks have triggered the shifts from drought to pluvial conditions since 1980. *Commun. Earth Environ.* 4 (1), 254.
- Ramamurthy, P., González, J., Ortiz, L., Arend, M., Moshary, F., 2016. Impact of heatwave on a megacity: an observational analysis of new york city during july 2016. *Environ. Res. Lett.* 12 (5), 54011. <https://doi.org/10.1088/1748-9326/aa6e59>.
- Rastogi, A., Antala, M., Bka, M.G.K.A., Ski, S.L.A., Rosadzi N., Ecki, M. Str.O.Z., Brestic, M., Juszczak, R.L.A., 2020. Impact of warming and reduced precipitation on morphology and chlorophyll concentration in peat mosses (sphagnum angustifolium and s. Fallax). *Sci. Rep.* 10 (1), 1–9. <https://doi.org/10.1038/s41598-020-65032-x>.
- Rohini, P., Rajeevan, M., Srivastava, A.K., 2016. On the variability and increasing trends of heat waves over India. *Sci. Rep.* 6 (1), 1–9. <https://doi.org/10.1038/srep26153>.
- Scalley, B.D., Spicer, T., Jian, L., Xiao, J., Nairn, J., Robertson, A., Weeramanthri, T., 2015. Responding to heatwave intensity: excess heat factor is a superior predictor of health service utilisation and a trigger for heatwave plans. *Aust. N. Z. J. Public Health* 39 (6), 582–587. <https://doi.org/10.1111/1753-6405.12421>.
- Sinha, P., Coville, R.C., Hirabayashi, S., Lim, B., Endreny, T.A., Nowak, D.J., 2022. Variation in estimates of heat-related mortality reduction due to tree cover in us cities. *J. Environ. Manag.* 301, 113751.
- Steeneveld, G.J., Koopmans, S., Heusinkveld, B.G., Theeuwes, N.E., 2014. Refreshing the role of open water surfaces on mitigating the maximum urban heat island effect. *Landscape Urban Plan.* 121, 92–96. <https://doi.org/10.1016/j.landurbplan.2013.09.001>.
- Szagri, D., Nagy, B., Szalay, Z., 2023. How can we predict where heatwaves will have an impact? – a literature review on heat vulnerability indexes. *Urban Clim.* 52, 101711 <https://doi.org/10.1016/j.uclim.2023.101711>.
- Taleghani, M., Kleerekoper, L., Tenpierik, M., Van Den Dobbelaer, A., 2015. Outdoor thermal comfort within five different urban forms in the Netherlands. *Build. Environ.* 83, 65–78. <https://doi.org/10.1016/j.buildenv.2014.03.014>.
- Teuling, A.J., Seneviratne, S.I., St O Ckli, R., Reichstein, M., Moors, E., Ciais, P., Luyssaert, S., et al., 2010. Contrasting response of european forest and grassland energy exchange to heatwaves. *Nat. Geosci.* 3 (10), 722–727. <https://doi.org/10.1038/ngeo950>.
- Tripathy, K.P., Mishra, A.K., 2023. How unusual is the 2022 european compound drought and heatwave event? *Geophys. Res. Lett.* 50 (15), e2023G-e105453G. <https://doi.org/10.1029/2023GL105453>.
- Wang, J., Yan, Z., 2021. Rapid rises in the magnitude and risk of extreme regional heat wave events in China. *Weather Clim. Extrem.* 34, 100379.
- Wang, Y., Lu, B., Han, Z., 2023. Rapid increase of the nighttime electricity demand in Beijing due to compound heatwaves. *Urban Clim.* 50, 101595 <https://doi.org/10.1016/j.uclim.2023.101595>.
- Wong, M.S., Yang, J., Nichol, J., Weng, Q., Menenti, M., Chan, P.W., 2015. Modeling of anthropogenic heat flux using hj-1b chinese small satellite image: a study of heterogeneous urbanized areas in Hong Kong. *IEEE Geosci. Remote Sens. Lett.* 12 (7), 1466–1470. <https://doi.org/10.1109/LGRS.2015.2409111>.
- Xu, Z., Fitzgerald, G., Guo, Y., Jalaludin, B., Tong, S., 2016. Impact of heatwave on mortality under different heatwave definitions: a systematic review and meta-analysis. *Environ. Int.* 89, 193–203.
- Xu, T., Yao, R., Du, C., Li, B., 2023. Outdoor thermal perception and heatwave adaptation effects in summer – a case study of a humid subtropical city in China. *Urban Clim.* 52, 101724 <https://doi.org/10.1016/j.uclim.2023.101724>.
- Yang, J., Huang, X., 2021. The 30 m annual land cover dataset and its dynamics in China from 1990 to 2019. *Earth Syst. Sci. Data* 13 (8), 3907–3925. <https://doi.org/10.5194/essd-13-3907-2021>.
- Yu, C., Hien, W.N., 2006. Thermal benefits of city parks. *Energ. Build.* 38 (2), 105–120. <https://doi.org/10.1016/j.enbuild.2005.04.003>.
- Zauli Sajani, S., Tibaldi, S., Scotti, F., Lauriola, P., 2008. Bioclimatic characterisation of an urban area: a case study in bologna (Italy). *Int. J. Biometeorol.* 52 (8), 779–785. <https://doi.org/10.1007/s00484-008-0171-6>.
- Zhang, X., Chen, F., Chen, Z., 2023. Heatwave and mental health. *J. Environ. Manag.* 332, 117385 <https://doi.org/10.1016/j.jenvman.2023.117385>.
- Zhao, G., Gao, H., 2019. Estimating reservoir evaporation losses for the United States: fusing remote sensing and modeling approaches. *Remote Sens. Environ.* 226, 109–124. <https://doi.org/10.1016/j.rse.2019.03.015>.
- Zhou, W., Wang, L., Li, D., Leung, L.R., 2021. Spatial pattern of lake evaporation increases under global warming linked to regional hydroclimate change. *Commun. Earth Environ.* 2 (1), 1–10. <https://doi.org/10.1038/s43247-021-00327-z>.
- Zhou, W., Wang, Q., Li, R., Zhang, Z., Wang, W., Zhou, F., Ling, L., 2023. The effects of heatwave on cognitive impairment among older adults: exploring the combined effects of air pollution and green space. *Sci. Total Environ.* 166534 <https://doi.org/10.1016/j.scitotenv.2023.166534>.
- Zou, Z., Yan, C., Yu, L., Jiang, X., Ding, J., Qin, L., Wang, B., Qiu, G., 2021. Impacts of land use/land cover types on interactions between urban heat island effects and heat waves. *Build. Environ.* 204, 108138 <https://doi.org/10.1016/j.buildenv.2021.108138>.